

See discussions, stats, and author profiles for this publication at: <https://www.researchgate.net/publication/323630374>

Dopaminergic neuromodulation of high-gamma stimulus phase-locking in gerbil primary auditory cortex mediated by D1/D5-receptors

Article in European Journal of Neuroscience · March 2018

DOI: 10.1111/ejn.13898

CITATIONS

0

READS

102

6 authors, including:



Matthias Deliano

Leibniz Institute for Neurobiology

29 PUBLICATIONS 242 CITATIONS

[SEE PROFILE](#)



Michael G.K. Brunk

Leibniz Institute for Neurobiology

11 PUBLICATIONS 25 CITATIONS

[SEE PROFILE](#)



Mohamed El Tabbal

Okinawa Institute of Science and Technology

2 PUBLICATIONS 21 CITATIONS

[SEE PROFILE](#)



Maria-Marina Zempeltzi

Leibniz Institute for Neurobiology

2 PUBLICATIONS 1 CITATION

[SEE PROFILE](#)

Some of the authors of this publication are also working on these related projects:



Dopaminergic influence on cortical processing in actively behaving rodents by optogenetical stimulation of the ventral tegmental area
[View project](#)



Effects of the glycan polysialic acid on prefrontal cortex synaptic plasticity and learning [View project](#)

Dopaminergic neuromodulation of high gamma stimulus phase-locking in gerbil primary auditory cortex mediated by D1/D5-receptors

Matthias Deliano,^{1,†} Michael G. K. Brunk,^{1,†} Mohamed El-Tabbal,¹ Maria M. Zempeltzi,¹ Max F. K. Happel¹ and Frank W. Ohl^{1,2,3} 

¹Department Systems Physiology of Learning (SPL), Leibniz Institute for Neurobiology (LIN), Brenneckestr. 6, Magdeburg 39118, Germany

²Otto von Guericke University (OVGU), Magdeburg, Germany

³Center for Behavioral Brain Sciences (OVGU), Magdeburg, Germany

Keywords: oscillation, spectral analysis, time–frequency analysis, current source density, Mongolian gerbil

Abstract

Cortical release of the neurotransmitter dopamine has been implied in adapting cortical processing with respect to various functions including coding of stimulus salience, expectancy, error prediction, behavioral relevance and learning. Dopamine agonists have been shown to modulate recurrent cortico-thalamic feedback, and should therefore also affect synchronization and amplitude of thalamo-cortical oscillations. In this study, we have used multitaper spectral and time–frequency analysis of stimulus-evoked and spontaneous current source density patterns in primary auditory cortex of Mongolian gerbils to characterize dopaminergic neuromodulation of the oscillatory structure of current sources and sinks. We systemically applied D1/D5-receptor agonist SKF-38393 followed by competitive D1/D5-receptor antagonist SCH-23390. Our results reveal an increase in stimulus phase-locking in the high gamma-band (88–97 Hz) by SKF-38393, specifically in layers III/IV at the best frequency, which occurred at 20 ms after tone onset, and was reversed by SCH-23390. However, changes in induced oscillatory power after SKF-38393 treatment occurred stimulus-independently in the background activity in different layers than phase-locking effects and were not reversed by SCH-23390. These effects might either reflect longer-lasting changes in neural background noise, non-specific changes due to ketamine anesthesia, or an interaction of both. Without concomitant stimulus-induced power increase, increased stimulus phase-locking in layers III/IV indicates enhanced phase-resetting of neural oscillations by the stimulus after D1/D5-receptor activation. The frequency characteristics, together with the demonstrated stimulus specificity and layer specificity, suggest that changes in phase-resetting originate from dopaminergic neuromodulation of thalamo-cortical interactions. Enhanced phase-resetting might be a key step in the recruitment of cortical activity modes interpreting sensory input.

Introduction

Several studies have demonstrated that the release of the neurotransmitter dopamine (DA) in auditory cortex plays important roles for auditory learning in the context of stimulus detection and discrimination experiments (Schicknick *et al.*, 2008, 2012; Stark *et al.*, 2008; Rothe *et al.*, 2009). Generally, DA has been implicated in various signaling functions ranging from the coding of stimulus salience to the coding of expectations or their violations (prediction

errors) (for review, see Bromberg-Martin *et al.*, 2010). In a recent study, we have identified the recruitment of a DA-modulated recurrent cortico-efferent feedback loop as a mechanism underlying the improved detection of behaviorally relevant stimuli in auditory tasks (Happel *et al.*, 2014). This recruitment leads to a specific pattern of increased amplitudes of current sources and sinks in several layers of the auditory cortex. We hypothesize that gain modulation of this feedback loop will not only change early peaks in the evoked response, but also lead to a change in the temporally more extended oscillatory structure of the cortical response. Also, it is not clear whether DA-induced amplitude increases in a trial-averaged measure of activity, as is the case for the early CSD peaks in our previous work, reflect corresponding power increases in single-trial responses, or increased phase-locking to the stimulus, or a mixture of both. This is somewhat analogous to the discussion of whether the amplitude of a trial-averaged electric potential does more reflect modulation of power or phase structure of the underlying single-trial

Correspondence: Prof. Dr. Frank W. Ohl, as above. E-mail: frank.ohl@LIN-magdeburg.de

†Both authors contributed equally.

Received 30 June 2017, revised 1 March 2018, accepted 1 March 2018

Edited by Dr. Sophie Molholm. Reviewed by Andrei Popescu, Circuit Therapeutics Inc, USA; Matthew Albrecht, University of Maryland, USA; and Krishnan Padmanabhan, University of Rochester Medical Center, USA

All peer review communications can be found with the online version of the article.

responses. It should, however, be emphasized that the question of whether the DA-induced modulation of trial-averaged amplitudes reflects more single-trial power effects or single-trial phase-locking effects, is independent of the much debated question to which degree the trial-averaged signals themselves are reflecting power or phase characteristics (e.g., Min *et al.*, 2007).

Here, we investigate the contributing factors of the DA-induced increase in cortical current sources and sinks using multitaper spectral analysis of layer-specific CSD signals. CSD reconstruction from measured LFPs was chosen because it reduces blur of spatial profiles due to volume conduction and reduces spatial biases due to electric referencing. We employ multitaper spectral analysis, in order to obtain robust and unbiased estimates of power and phase, as well as time-frequency analysis to determine the time-course of the effects. At short latency after stimulus onset (20 ms), we demonstrate layer- and stimulus-specific antagonistic dopaminergic neuro-modulation of stimulus phase-locking in the high gamma-band of CSD signal from 88 to 107 Hz. Increased local thalamo-cortical synchronization in the high gamma-band (>60 Hz) might facilitate the recruitment of supragranular associative networks that give rise to spatiotemporal activity pattern carried by oscillations in the low gamma-band (Ohl *et al.*, 2001).

Materials and methods

All experiments were carried out in adult male Mongolian gerbils (*Meriones unguiculatus* (breed in house), age: 4–8 months, body weight: 75–100 g; $n = 8$). Experiments were conducted in accordance with ethical animal research standards defined by the German Law and approved by an ethics committee of the state Saxony-Anhalt, Germany.

Surgery and recordings

Surgical procedures were conducted as described in detail earlier (Happel *et al.*, 2014). Briefly, animals were anaesthetized by intraperitoneal perfusion (0.06 mL/h) of 45% ketamine (50 mg/mL, Ratiopharm), 5% xylazine (Rompun, 2%, BayerVital) and 50% isotonic sodium chloride solution (154 mmol/L, Braun). The implantation site for the CSD electrode in right primary auditory cortex AI was chosen based on anatomical landmarks and vascularization pattern. Subsequent recordings of physiological parameters like onset latencies and frequency tuning (Thomas *et al.*, 1993; Ohl *et al.*, 2000; Happel *et al.*, 2010) allowed determination of the here represented tone frequencies to confirm the electrode position in the tonotopic map (Radtke-Schuller *et al.*, 2016).

Experiments were performed in an acoustically and electrically shielded recording chamber. Depth profiles of local field potentials (LFP) were recorded using linear multichannel electrodes (Neuronexus A1x32-50-413) implanted perpendicular to the cortical layers with upper contact at the surface (cf. Happel *et al.*, 2010). Recorded LFPs were pre-amplified (500 \times), and band-pass filtered between 0.7 and 300 Hz (3 dB cutoff frequency) with a PBX2 preamplifier (Plexon Inc.). Signals were then digitized at 2 kHz with a multichannel-recording system (Multichannel Acquisition Processor, Plexon Inc.).

Pure tones (65 dB SPL, 200-ms duration, 5-ms cosine-squared onset- and offset-ramps) were delivered by a programmable attenuator (gPAH, Guger Technologies), an amplifier (STAX SRM-3) and an electrostatic headphone (STAX SR lambda professional) positioned 3 cm in front of the animal. Frequencies varied in the range from 125 to 32 kHz in octave steps. In each of a 100 repetitions,

frequencies, an acoustic click and a silent pause condition were randomized, and presented at an interstimulus interval of 800 ms. LFP recordings were continuously carried out through the experiments in 15-min blocks.

After insertion of the multi-electrode, we waited at least 30 min until auditory evoked responses of the initial baseline measurements (BL) were stable as determined from frequency-dependent evoked potentials, online (cf. Happel *et al.*, 2014). After 30–50 min, D1/D5-receptor agonist SKF-38393 (5 mg/kg; i.p.; Schicknick *et al.*, 2008) was applied. After 60–120 min recording under SKF-38393, we finally applied the competitive D1/D5-receptor antagonist SCH-23390 (0.1 mg/kg, dissolved in 0.9% sodium chloride) and continued recording for further 60–120 min. LFPs recorded within 10–20 min before SKF-38393 application were used as a baseline. Effects of SKF-38393 and SCH-23390 were determined from blocks of LFP-recordings between 30 and 90 min after injection. SKF-38393 was applied in eight animals, SCH-23390 in five of these animals.

Current source density analysis

Epochs from 200 ms before to 600 ms after tone- or pause onset were extracted from the LFPs. For each time-point in each epoch, a one-dimensional current source density (CSD) profile was derived from the second spatial derivative of the LFPs as follows (Fig. 1):

$$-\text{CSD} \approx \frac{\delta^2 \phi(z)}{\delta z^2} = \frac{\phi(z + n\Delta z) - 2\phi(z) + \phi(z - n\Delta z)}{(n\Delta z)^2}$$

where ϕ represents the electric field potential, z is the spatial coordinate perpendicular to the cortical layers, Δz is the spatial sampling interval (50 μm), and n is the differentiation grid (Mitzdorf, 1985; Happel *et al.*, 2010). LFP profiles were smoothed with a weighted average (Hamming window) across seven channels (spatial filter kernel of ~300 μm). To retain the upper and lower boundary sites, we used a linear extrapolation method that assumes no additional decay in the second derivative of the field potential (Happel *et al.*, 2010).

Current source density profiles (Fig. 1) were used to define the cortical layers. Canonical CSD patterns allow for identifying early granular and infragranular sinks, which are less affected by superposition than later sources and sinks. These sinks have been shown to reflect thalamic input into layers III-IV and Vb, respectively (Happel *et al.*, 2010). Using these sinks, we determined layers III-IV and Vb in each animal. Based on these layers, we then defined layers I-II as the layers above III-IV, layer Va as the layer between III-IV and Vb, and layer VI as the layer below Vb. We restricted the layers to the radial extent of the sinks in each layer. CSD traces within these layers were averaged across the channels belonging to the layer. The number of channels per individual sink component was kept constant when comparing responses across treatments and was largely similar across animals (Happel *et al.*, 2014).

Data selection

Analysis was carried out for different stimulus conditions: best frequency (BF), non-best frequency (non-BF) and without stimulation (pause). To determine the best frequency of the recording site in an animal, response curves as a function of tone frequency, RMS amplitudes of the CSD signals from layers III/IV were calculated within a 60-ms time window after stimulus onset. BFs were defined as the frequency of maximum RMS amplitude for each subject and

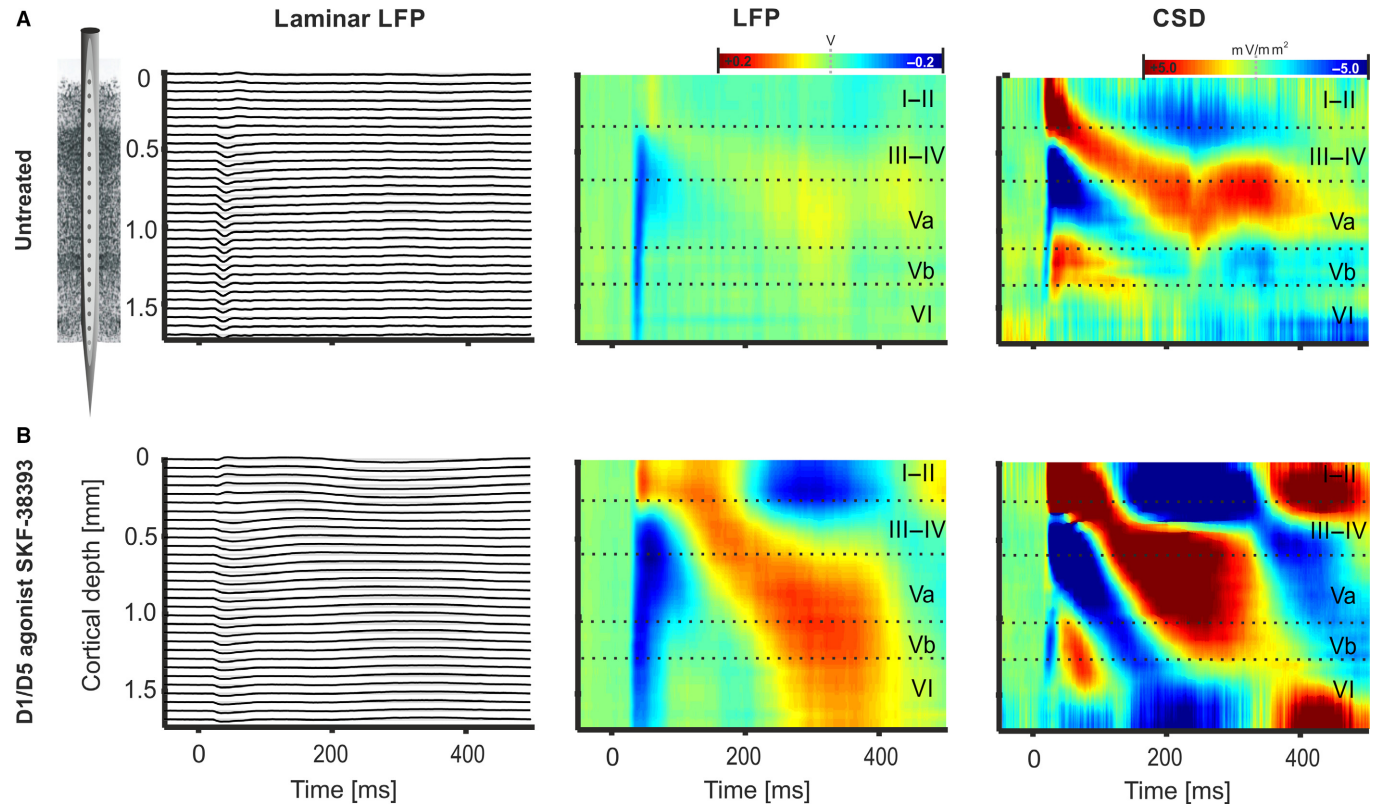


FIG. 1. Representative example of averaged evoked potentials in response to BF stimulation at the 32 recording channels of the radial shaft electrode (left column), laminar profiles of evoked potentials (second column) and current source density (CSD) distributions derived as cross-laminar second spatial derivative of the potentials from the baseline BL measurement (A) and after injection (i.p.) of D1/D5-receptor agonist SKF-38393 (B).

pharmacological treatment (see Fig. S1B). For the BF condition, results (see below) were averaged across the two frequencies with largest RMS amplitudes in each subject, to increase robustness. For the non-BF condition, results were averaged across frequencies adjacent to the BFs, at a distance of maximally two octaves.

Spectral analysis of CSD data

Traditional Fourier spectral analysis uses a single windowing function (taper) chosen by the analyst. Spectral estimates based on these single-window transforms have large variance and are biased especially at higher frequencies. We therefore used a multitaper Fourier transform, which employs multiple tapers that are orthogonal to each other. Analysis was carried out with the MATLAB-based Chronux toolbox (<http://chronux.org>) implementing this multitaper method. Single-trial CSD signals were transformed into the frequency domain by a multitaper fast Fourier transform within 800 ms epochs from -200 to 600 ms relative to stimulus/pause onset. We employed five tapers of 800 ms length with a time-bandwidth product of 3 and no zero-padding (Mitra & Bokil, 2008; Bokil *et al.*, 2010). To obtain the stimulus-evoked power spectrum, that is, the spectrum of the averaged evoked CSD signal, we averaged the complex valued spectra across trials before calculating the power as squared magnitude of the average. This is equivalent to calculating the spectrum of the trial-averaged signals. To homogenize variances, power spectra were log-transformed. To quantify the phase-locking to the stimulus onset independent of the response amplitude, we calculated a phase-locking index across trials. For this, we normalized at each frequency the complex valued transformation by its

magnitude and then averaged the resulting phase vectors across trials. If an oscillatory response to a stimulus has the same phase across trials, this index attains a value of 1 at its spectral frequency. For the analysis of pure amplitude effects, that is, changes in power independent of the phase-locking and temporal jitter across trials, we obtained an induced power spectrum by calculating the logarithm of the power spectrum of each single trial before averaging across trials. As induced spectra might include background effects unrelated to stimulus, we further calculated a stimulus-induced power spectrum relative to silent background by subtracting the induced logarithmic spectrum of the pause condition from the induced spectra of the tone responses.

By comparing stimulus-induced power and phase-locking index, phase-resetting of oscillations by a stimulus can be dissociated from amplitude changes in response to stimulation. All spectra were smoothed with a bandwidth of two frequency points. Finally, the mean and the standard error of the mean of the power spectra and the phase-locking indices were calculated across subjects and tapers.

Statistical analysis of spectra

We compared all spectra before and after administration of SKF-38393, and after subsequent administration of SCH-23390 across subjects and tapers, separately for each stimulus condition (BF, non-BF, pause) and layer (I/II, III/IV, Va, Vb, VI). Comparisons were restricted to a frequency range from 3 to 300 Hz. The lower cutoff guaranteed that the analysis was based on at least three cycles given the length of the analysis window (800 ms), and the upper cutoff frequency was limited by the recording system (see above). As the

phase-locking index is bounded between 0 and 1, phase-locking spectra were normalized by a logistic transformation prior to further analysis.

Then, *t*-scores were calculated for the comparisons between BL and SKF-38393, and between SKF-38393 and SCH-23390 for each spectrum, frequency, stimulus condition, and layer using sample mean and variance. We then applied a permutation test (Groppe *et al.*, 2011) by randomly exchanging pairs of observations 1000 times and calculating the *t*-scores for each frequency and permutation. To correct for multiple testing across frequencies, we only selected the most extreme *t*-value (maximum or minimum) across frequencies in each permutation (*t*_{extreme}). A *P*-value was estimated by determining the ratio of extreme *t*-values above or below the actually observed *t*-values in the spectrum across permutations. For the test decision, α -levels were further Bonferroni-corrected for multiple testing in each of the five layers.

Time-frequency analysis

In selected layers, frequency bands and stimulus conditions displaying significant effects in multitaper spectral analysis, we further carried out time-frequency analysis. CSD signals, epoched from −1400 to 1600 ms relative to stimulus onset, were band-pass filtered in frequency bands showing significant effects using a digital Parks-McClellan finite impulse response (FIR) filter. Filter order ranged from 1000 to 54 and was adapted such that it entailed three (<8 Hz) to six (>8 Hz) cycles of the lower cutoff frequency of the filter band. After filtering, a Hilbert transform was applied to obtain the analytic signal. The analytic signal was down-sampled from 1000 to 100 Hz and smoothed by a moving window average with a window length of 10 points. For each time-point, analytic power and phase-locking values were then calculated as described for the multitaper spectra. For statistical analysis of selected frequency bands and layers, log-transformed analytic power and logit-transformed phase-locking values were averaged in a pre-stimulus (−200 to −50 ms) interval, an early (0–50 ms) and a late (50–400 ms) post-stimulus interval. Statistical *t*-values were calculated for the comparisons of SKF-38393 treatment versus BL and SCH-23390 versus SKF-38393 treatments across those subjects treated with both substances ($n = 5$). Permutation testing of modulation effects was carried out for the contrast between these treatment effects for the log-transformed power or logit-transformed phase-locking values in the three intervals, and with Bonferroni correction to account for multiple testing.

Results

Cortical auditory evoked potentials in response to pure-tone stimulation display layer-dependent amplitude- and frequency-modulated oscillations. In the present work, we analyzed whether and how the generators of the cortical oscillations determined by CSD analysis are modulated by dopamine in different cortical layers. For this, we carried out a layer-specific multitaper spectral analysis of CSD responses to pure tones and investigated their dopaminergic modulation in the frequency domain.

The right column of Fig. 1 shows representative CSD responses at the best frequency (BF) for the baseline (BL, Fig. 1A), and after systemically applied D1/D5-receptor agonist SKF-38393 (Fig. 1B). CSD distributions originate from a superposition of sources and sinks in space and time, and display a canonical spatiotemporal pattern in correspondence to the anatomical layers of auditory cortex (Happel *et al.*, 2010). Based on this pattern, we defined layers I-II,

III-IV, Va, Vb and VI as described in the Methods sections and averaged CSD signals across channels within these layers. Notably, CSD is a measure of synaptic mass current and is less distorted by volume conduction as compared to the local field potential (LFP). Therefore, layer-averaged CSD signals are expected to be spatially more confined than layer-averaged LFPs (Mitzdorf, 1985). For a representative example of the CSD patterns after stimulation with non-BF stimuli, see Fig. S1.

Evoked and induced power spectra

First, we compared the power spectrum of the averaged evoked CSD signal in each layer (*evoked spectrum*), and the average across the power spectra of each single-trial CSD signal (*induced spectrum*). Whereas the former reflects a mixture of changes in amplitude and stimulus phase-locking, the latter quantifies changes in amplitude independent of phase jitter across trials. Figure 2 shows the grand mean and standard error of the evoked (A) and the induced (B) spectra of the CSD responses in the different cortical layers for the baseline (BL, green), with agonist SKF-38393 (red) and after subsequent treatment with antagonist SCH-23390 (blue) during BF stimulation. Red asterisks mark significant changes ($P < 0.050$) from BL to SKF-38393, and green asterisks from SKF-38393 to SCH-23390 (see below, and Fig. 3). Each column of panels displays data from a different layer. As it is typical for cortical population signals, power in all layers and for all treatments decays without larger spectral peaks almost linearly in a double logarithmic coordinate system across frequencies above 10 Hz (Freeman *et al.*, 2006). Differences between pharmacological conditions can be found over broad frequency ranges below 60 Hz. More confined changes in frequency space occur with pharmacological treatment at lower (<10 Hz) frequencies of evoked and induced spectra in layer VI, and at higher (>70 Hz) frequencies in the evoked spectra of layers III/IV. A proper interpretation of these diverse spectral changes requires statistical analysis. Figure 3 shows for BF stimulation and for different layers, the *t*-values of evoked (black) and induced (green) spectra contrasting BL with SKF-38393 (A), and SCH-23390 with SKF-38393 (B), respectively. Statistical *t*-values were calculated as the mean spectral differences between these pharmacological conditions across subjects ($n = 8$ for SKF-38393 vs. BL, and $n = 5$ for SCH-23390 vs. SKF-38393) and tapers ($n_t = 5$) normalized by their standard error (SEM). Significant differences were determined by a permutation test correcting *P*-values for multiple testing by selecting absolute *t*-value maxima across frequencies in each permutation, and by additional Bonferroni correction of significance levels (see Methods).

Our aim was to find reverse effects of agonist SKF-38393 and subsequent antagonist SCH-23390 treatment. In layers III/IV application of SKF-38393 increased evoked power (Fig. 2A) in the high gamma-band with respect to BL, significantly in a range of 89–96 Hz by about +4.1 SEM ($P = 0.009$, black asterisks in second panel of Fig. 3A). The sharp positive *t*-value peak in Fig. 3A indicates that the maximum of the effect occurred at 94 Hz. Antagonist SCH-23390, on the other hand, decreased evoked power with respect to SKF-38393 in the same layer in an overlapping frequency range, significantly between 85 and 111 Hz by about −4.8 SEM ($P = 0.013$, black asterisks in second panel of Fig. 3B). The maximum effect also peaked around 94 Hz.

In layers I/II, SKF-38393 administration also leads to a significant increase in the evoked high gamma power by about +5.2 SEM vs. BL ($P = 0.010$, 75–89 Hz, black asterisks in first panel of Fig. 3A), although without corresponding decrease after application of

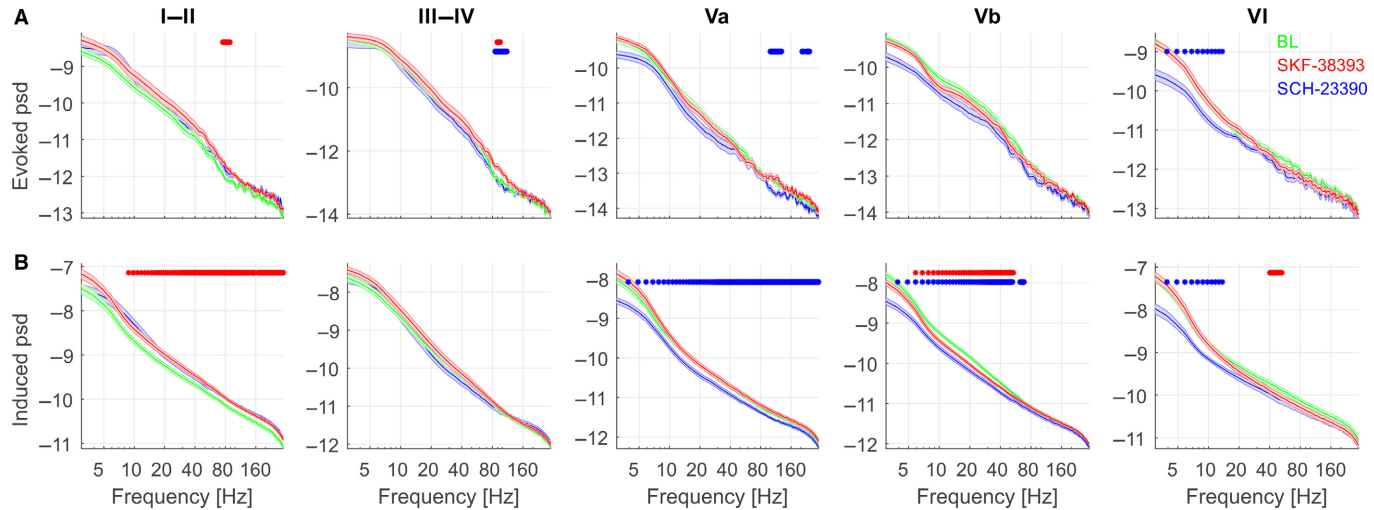


FIG. 2. Multitaper frequency spectra of epochs from -200 to 600 ms relative to stimulus onset at the best frequency. (A) Evoked power spectrum of layer-specific trial-averaged CSD signals and (B) induced power spectrum as average of the power spectra of single-trial layer-specific CSD signals. Power spectra are shown for baseline (BL; green), before administration of D1/D5-receptor agonist SKF-38393 (red) and after administration of D1/D5-receptor antagonist SCH-23390 (blue). Shown are the grand mean and standard errors of the logarithmic spectra across subjects ($n = 8$ for BL and SKF-38393, $n = 5$ for SCH-23390) and tapers ($n_t = 5$). Spectra are displayed on double logarithmic scales. Significant differences obtained from permutation testing (see Fig. 3) between SKF-38393 and BL, and between SCH-23390 and SKF-38393, were marked by red and green asterisks, respectively. In this and following figures, panels in a row present the results from left to right for layers I-II, III-IV, Va, Vb and VI.

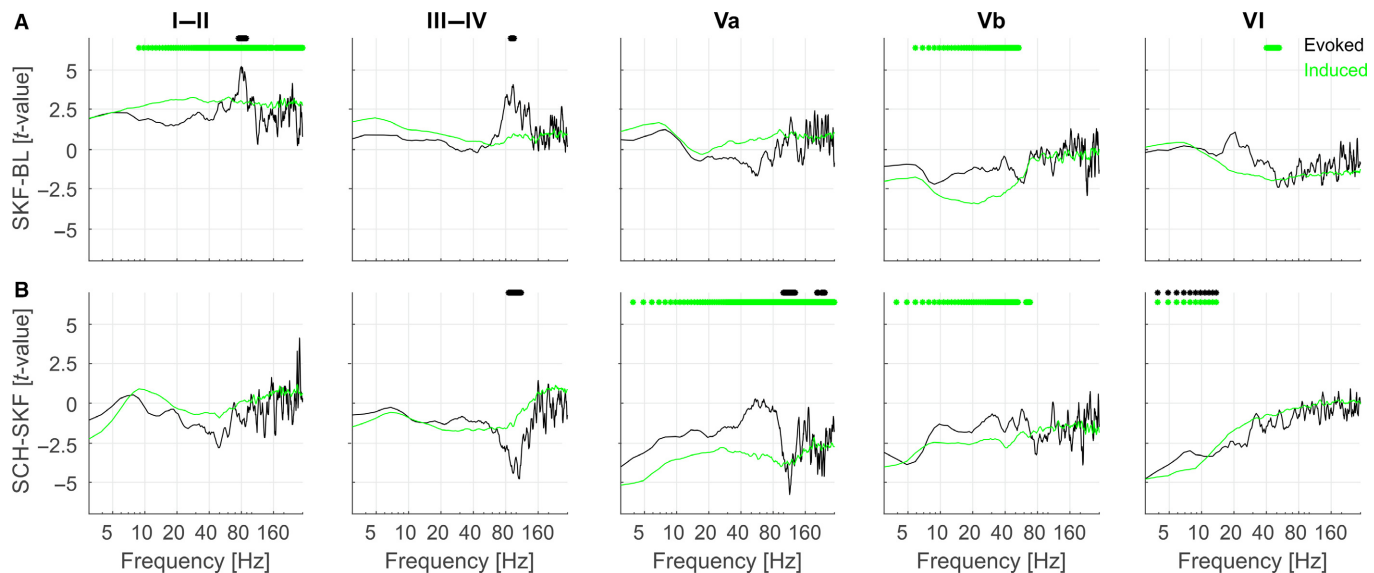


FIG. 3. Standardized differences of evoked (black), and induced power spectra (green) between SKF-38393 and BL (A), and between SCH-23390 and SKF-38393 expressed as t -values. Power spectra were log-transformed for each taper on the single-trial level. Standardization was based on sample means and standard errors of the mean across subjects ($n = 8$ for BL vs SKF-38393, $n = 5$ for SCH-23390 vs SKF-38393) and tapers ($n_t = 5$). Asterisks mark Bonferroni-corrected significant differences in the corresponding color. For details, see Materials and Methods.

antagonist SCH-23390 (first panel in Fig. 3B). Decreases only with antagonist SCH-23390 by -4.8 to -5.8 SEM vs. SKF-38393 were found in the high gamma-band between 100 and 244 Hz in layer Va ($P = 0.006$, $100\text{--}121$ Hz, $123\text{--}129$ Hz, $206\text{--}212$ Hz, $226\text{--}234$ Hz and $237\text{--}244$ Hz, black asterisks in third panel of Fig. 3B), and at low frequencies in layer VI (-4.8 SEM, $P = 0.006$, $3\text{--}14$ Hz, black asterisks in fifth panel of Fig. 3B). Importantly, no significant changes were found during non-BF stimulation and pause (Fig. S3).

Changes in induced power (Fig. 2B) were distributed over broad frequency ranges and were smaller in size (3–4 SEM) than the

changes in evoked power. Whereas after SKF-38393-induced power was increased in layers I/II significantly at frequencies >10 Hz against BL ($P = 0.008$, green asterisks in first panel of Fig. 3A), it was decreased in infragranular layers Vb ($P = 0.014$, $6\text{--}54$ Hz, green asterisks in fourth panel of Fig. 3A), and VI ($P = 0.008$, $40\text{--}53$ Hz, green asterisks of fifth panel in Fig. 3A). However, after application of antagonist SCH-23390 these effects were not reversed, but a further decrease in induced power was found in infragranular layers. In layer Va, a broad power reduction was observed at all frequencies ($P = 0.005$, $3\text{--}300$ Hz, green asterisks of third panel in Fig 3B), and at lower frequencies in layer Vb

($P = 0.005$, 3–53 Hz, and 63–68 Hz, green asterisks in fourth panel of Fig. 3B) with SCH-23390 vs. SKF-38393. In layer VI, induced theta-/alpha-power was decreased at even lower frequencies from 3 to 14 Hz ($P = 0.002$, green asterisks in fifth panel of Fig. 3B). An almost identical pattern of induced power changes was found in response to non-BF stimulation (Fig. S2, light green curves and asterisks) and during the pause condition (Fig. S2, dark green curves and asterisks): A corresponding Broadband supragranular power increase, and infragranular power decrease at frequencies >10 Hz, was found with agonist SKF-38393 vs. BL ($P = 0.012$), and further infragranular power decreases occurred broadly in layer V and at lower frequencies (<15 Hz) in layer VI with antagonist SCH-23390 vs. SKF-38393 ($P = 0.017$). Thus, dopaminergic neuromodulation of induced power affected broad frequency bands and was not dependent on stimulation. Occurring even during the pause condition, the observed effects are probably due to an amplitude change in background oscillations. Broadband changes might thereby reflect changes in neural background noise.

Layer- and stimulus-specific dopaminergic modulation of stimulus phase-locking and relative induced power in the high gamma-band above 60 Hz

Notably, whereas evoked spectral changes can reflect changes in stimulus phase-locking, as well as changes in oscillatory response amplitude, induced power can reflect phase-independent changes in oscillatory response amplitude, but also changes in stimulus-independent background oscillations. To disambiguate the contribution of phase-locking across trials to the evoked spectra, we additionally analyzed spectra of the phase-locking index, that is, the trial average of the phase spectrum normalized to unit spectral amplitude. To disentangle neuromodulatory effects on the spontaneous oscillatory activity and on oscillatory stimulus responses, induced power spectra were normalized to the induced spectra of the pause condition yielding a *stimulus-induced power spectrum* relative to a silent background.

In contrast to the evoked and induced spectra, stimulus phase-locking (Fig. 4A) and induced relative power (Fig. 4B) spectra all showed a clear peak localized in the theta- or beta-band with maxima at around 7–20 Hz reflecting the frequency composition of the oscillatory CSD responses to the tone stimuli.

As shown in Fig. 5A, SKF-38393 led to a significant increase in stimulus phase-locking (second panel of Fig. 4A) across trials in a frequency range of 77–97 Hz (+4.2 to 5.7 SEM, $P = 0.008$, red asterisks in second panel in Fig. 5A). As can be seen from the *t*-values in Fig. 5A, this positive effect peaked at 93 Hz. Application of antagonist SCH-23390 selectively reversed this effect (blue asterisks in second panel of Fig. 4A), that is, significantly reduced phase-locking in the frequency range between 88 and 108 Hz (−4.0 to −5.5 SEM, $P = 0.006$, 88–97 Hz, and 99–108 Hz, red asterisks in second panel of Fig. 5B). Like the positive effect, this negative effect peaked around 93 Hz. Reduction in phase-locking by SCH-23390 in layers III–IV, but not its increase with SKF-38393, was accompanied by a decrease in stimulus-induced power (second panel of Fig. 4B) between 62 and 100 Hz by about −4.3 SEM ($P = 0.007$, 62–88 Hz, and 90–100 Hz, blue asterisks in second panel of Fig. 5B). Neither SKF-38393 nor SCH-23390 changed stimulus phase-locking or stimulus-induced relative power in other frequency bands, other layers, neither in response to BF nor to non-BF stimulation, or during the pause condition (Fig. S3).

Altogether, these results demonstrate a highly layer- and stimulus-specific antagonistic dopaminergic neuromodulation of high gamma

stimulus phase-locking in layers III/IV, only after BF stimulation. Stimulus phase-locking largely explained the observed changes of evoked high gamma power in layers III/IV by dopaminergic neuromodulation (compare black curves in Fig. 3 with red curves in Fig. 5).

Stimulus-dependent tuning of neuromodulatory effects

We then determined the tuning of the observed effects to stimulus frequency, in more detail. We obtained for each treatment response curves for early CSD amplitude, and for stimulus-evoked, and stimulus-induced high gamma power in layers III/IV as function of tone frequency. Response curves were aligned across subjects at the tone frequency of maximum response, that is, at the BF of the response. Before averaging across subjects, aligned response curves were normalized by subtracting the minimum and by dividing by the maximum range across stimuli and treatments in each subject.

Figure 6A shows the grand mean of normalized stimulus phase-locking values averaged in the band 88–107 Hz in layer III/IV as a function of distance to BF. Phase-locking is sharply tuned around BF, particularly after administration of SKF-38393 (red curve). At BF and 1 octave above BF, high gamma stimulus phase-locking was increased by agonist SKF-38393 vs. BL (red curve of phase-locking values in Fig. 6A, and red curve of *t*-values in Fig. 6D), an effect that was reversed after administration of antagonist SCH-23390 (blue curves in Fig. 6A and D). Statistically comparing the difference SKF-38393 vs. BL with SCH-23390 vs. SKF-38393, using a permutation test correcting for multiple testing across stimulus frequencies, revealed a significant antagonistic dopaminergic neuromodulation effect at BF and 1 octave above ($P = 0.020$, black asterisks in Fig. 6D). Weaker effects were found for stimulus-induced power (Fig. 6B, $P = 0.004$ at 1 octave above BF, asterisks in Fig. 6E), which showed broader tuning and a stronger reduction in amplitude by SCH-23390 than the original increase after administration of SKF-38393. Still a significant neuromodulatory effect was found 1 octave above BF. The root-mean-squared amplitude of the layers III/IV CSD time signal within the first 50 ms itself (Fig. 6C and F) also displayed tuning, but no significant neuromodulatory effects.

Time-frequency analysis of amplitude and phase effects

To determine the time-course of the neuromodulatory effects, we carried out a time-frequency analysis (see Methods) for the frequency bands, layers and stimulus conditions showing significant effects in multitaper spectral analysis. Figure 7A shows the time-courses of high gamma phase-locking determined for the frequency range from 88–107 Hz in which effects of SKF-38393 and SCH-23390 overlap. Phase-locking displays a maximum at 20 ms after stimulus onset. Only at the peak, phase-locking was increased from 0.1 at baseline (green curve) to 0.23 after SKF-38393 treatment (red curve), and back to the baseline level of 0.1 after administration of SCH-23390 (blue curve). Statistical *t*-values of mean phase-locking values within a pre-stimulus (−200 to −50 ms), an early (0 to 50 ms) and a late (50 to 400 ms) time window contrasting SKF-38393 vs. BL (red bars in Fig. 7E), and SCH-23390 vs. SKF-38393-BL (blue bars), respectively, showed large opposite effects within the early time window 0 to 50 ms after stimulus onset covering the peak, but not within the other time windows. A permutation test of *t*-values between SKF-38393 and SCH-23390 was significant for mean phase-locking values within the early time window ($P = 0.023$, black asterisk in Fig. 7E). No significant effects were

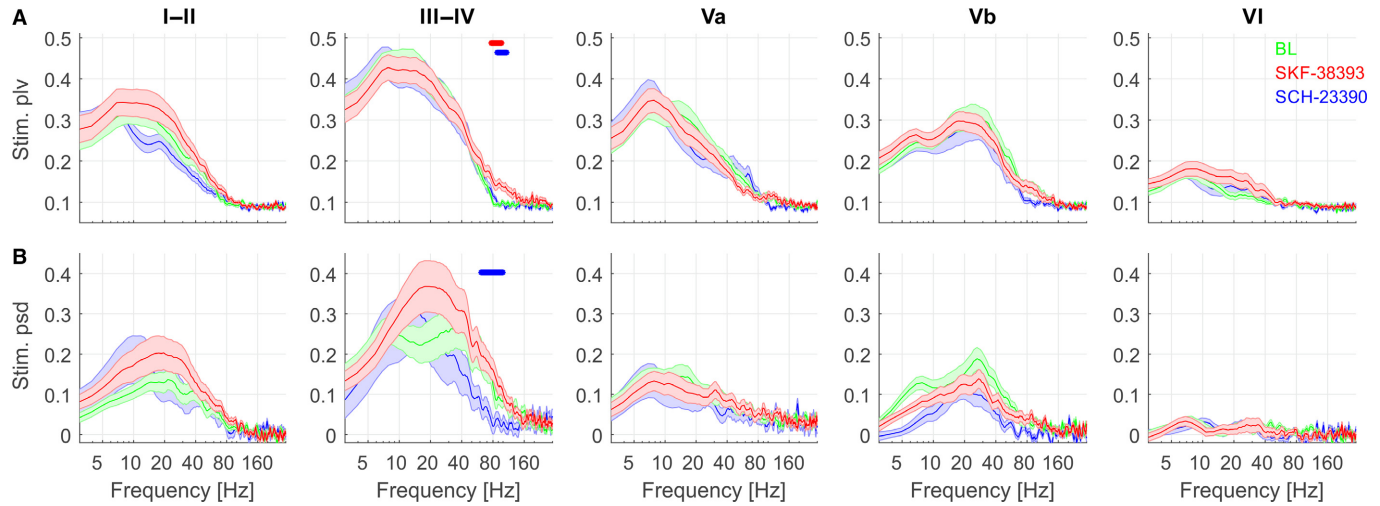


FIG. 4. Multitaper estimates of stimulus phase-locking and stimulus-induced power spectra from epochs -200 to 600 ms relative to stimulus onset at the best frequency (BF). (A) Stimulus phase-locking spectrum: average of amplitude-normalized phase vectors across trials. (B) Stimulus-induced power spectrum relative to background: induced power spectrum of tone stimuli relative to the induced spectrum of the pause condition. Induced power spectra were log-transformed prior to analysis. Therefore, relative spectra were calculated as difference between stimulus spectra and pause spectra. Baseline (BL) power spectra (green), spectra after administration of D1/D5-receptor agonist SKF-38393 (red) and after administration of D1/D5-receptor antagonist SCH-23390 (blue) are shown as grand mean and standard errors of the spectra across subjects ($n = 8$ for BL and SKF-38393, $n = 5$ for SCH-23390) and tapers ($n_t = 5$). Significant differences obtained from permutation testing (see Fig. 5) between SKF-38393 and BL, and between SCH-23390 and SKF-38393, were marked by red and blue asterisks, respectively.

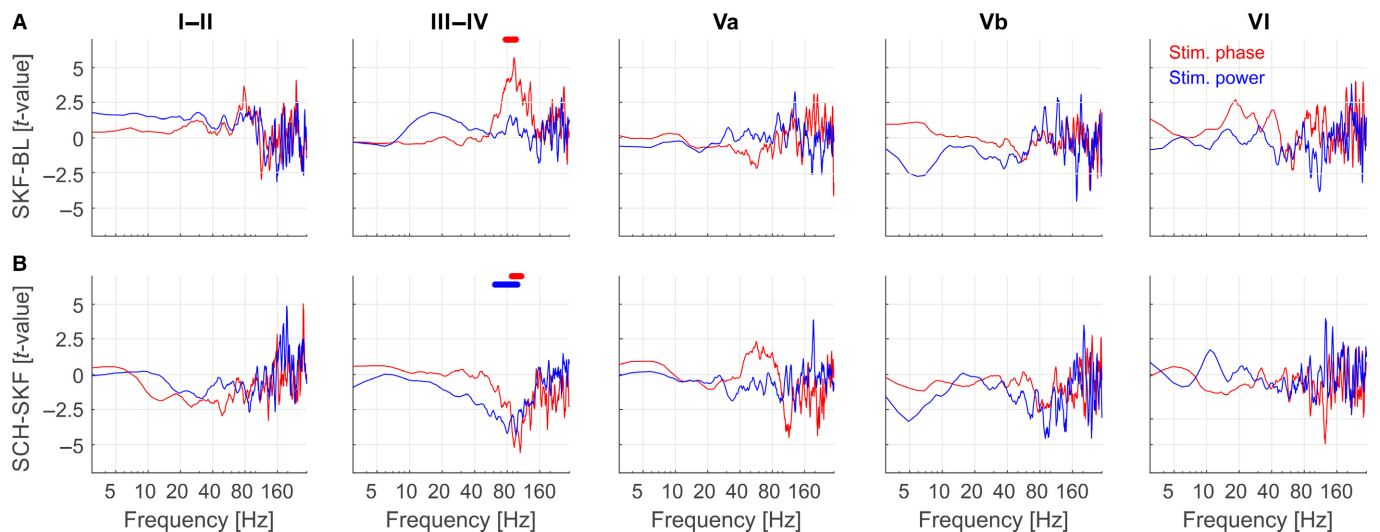


FIG. 5. Standardized differences of stimulus phase-locking (red), and stimulus-induced power (blue) spectra between SKF-38393 and BL (A), and between SCH-23390 and SKF-38393 expressed as t -values (B). Power spectra were log-, and phase-locking spectra logit-transformed for each taper, on the single-trial and on the single-subject level. Standardization was based on sample means and standard errors of the mean across subjects ($n = 8$ for BL vs SKF-38393, $n = 5$ for SCH-23390 vs SKF-38393) and tapers ($n_t = 5$). Asterisks mark Bonferroni-corrected significant differences in the corresponding color. For details, see Materials and Methods.

found for non-BF stimulation (Fig. 7F). Stimulus-induced power in the high gamma-band between 62 and 100 Hz also showed a maximum peak at a latency of 20 ms (Fig. 7C). Although the peak was slightly higher after SKF-38393 administration and decreased after SCH-23390 application, this effect in the early time window covering the peak was not significant. Notably, time-frequency analysis has less statistical power than multitaper spectral analysis. Demonstration of significant time-frequency effects would therefore require an increase in number of tested animals. Figure 7D shows the time-course of evoked high gamma power in the 88 – 107 Hz band with a peak maximum at 40 ms, that is, a longer latency than that of the

phase-locking peak in the same band. As with high gamma phase-locking, the peak increased after SKF-38393 and was reversed to baseline after SCH-23390 treatment, with a significant difference between mean evoked power values of these treatments within the early 0 – 50 ms post-stimulus time window ($P = 0.035$, Fig. 7H).

Figure 8 shows changes in the time-course of induced power occurring with dopaminergic neuromodulation within frequency bands of significant spectral effects. Induced power time-courses showed a peak maximum as well; however, differences between pharmacological treatments appeared as offsets largely constant over time, and without the reversal of SKF-38393 effects by SCH-23390.

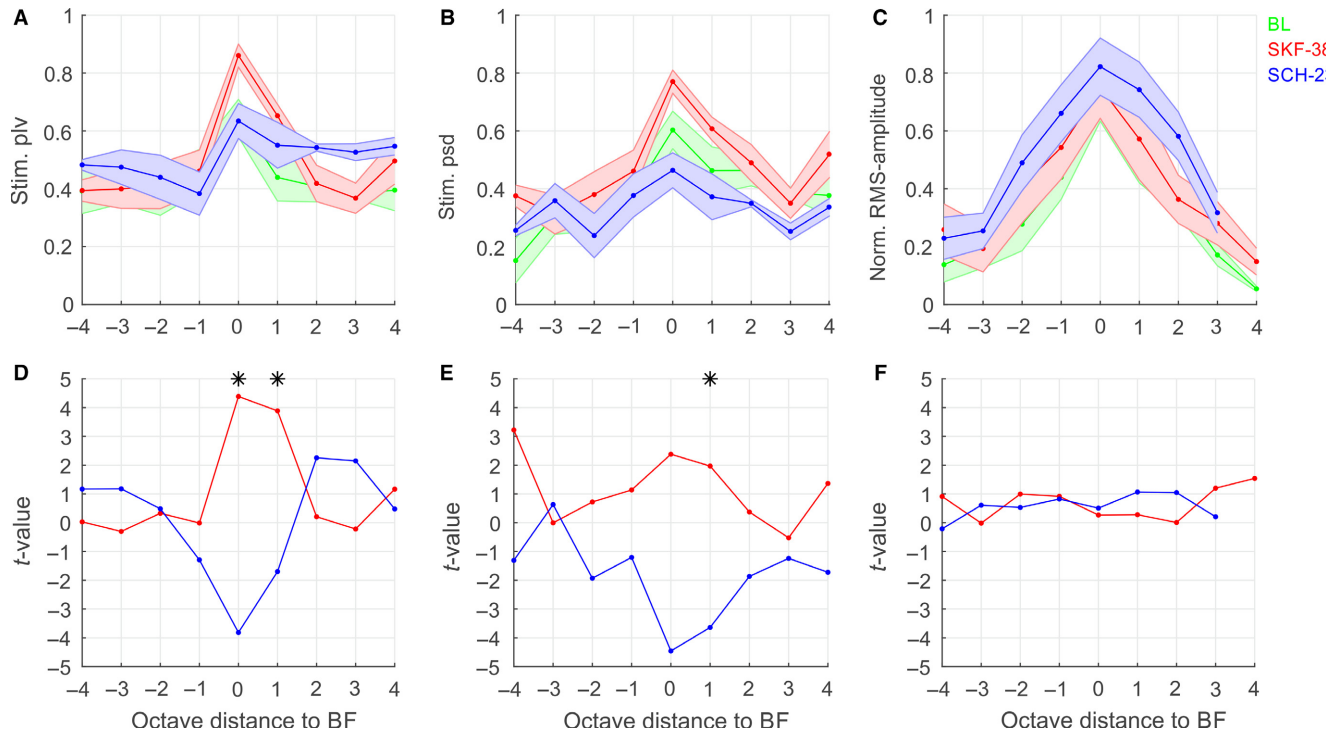


FIG. 6. Tuning of effects to stimulus frequency. Grand mean and standard errors of normalized response curves are shown as a function of octave distance of the stimulation tone frequency to BF at the recording site: (A) high gamma phase-locking values as median between 88 and 97 Hz. Values were normalized subject-wise to the maximum across pharmacological treatments, and aligned at the BF, that is, at the maximum for each treatment. (B) High gamma stimulus-induced relative power values as median between 62 and 100 Hz (normalization and alignment as in A). (C) RMS amplitudes of CSD signals in the first 50 ms after stimulus onset in layers III/IV (normalization and alignment as in A). Response curves for BL are shown in green, after SKF-38393 administration in red, and after SCH-23390 administration in blue. Statistical t-values of SKF-38393 vs. BL (red) and SCH-23390 vs. SKF-38393 (blue) for normalized and aligned high gamma stimulus phase-locking (D), high gamma stimulus-induced power (E) and RMS amplitude of early (0–50 ms) CSD in layer IV. Asterisks indicate significant neuromodulatory effects of the contrast (SKF-38393–BL)–(SCH-23390–KF-38393).

Even if not significant, effects of SKF-38393 and SCH-23390 were identical for pre-stimulus, and for early and late post-stimulus time windows. Observed induced power offsets were consistent with the observed significant increases and decreases in induced spectral power estimated by multitaper analysis.

Discussion

In the present study, we found that D1/D5-receptor agonist SKF-38393 increased stimulus phase-locking in the high gamma-band between 77 and 97 Hz with a sharp peak at 93 Hz as a response to BF stimulation. No such effect was found in response to stimulus frequencies more than 1 octave away from BF. Moreover, although CSD patterns are complex and contributing sources and sinks often span several cortical layers (Happel *et al.*, 2010; Schaefer *et al.*, 2017), dopaminergic neuromodulation of stimulus phase-locking occurred only in layers III/IV. In time, this effect showed a sharp peak with a maximum at 20 ms after stimulus onset. Most importantly, this effect was specifically reversed between 88 and 97 Hz by application of the competitive D1/D5-receptor antagonist SCH-23390, again with a peak of this negative effect at 93 Hz. Thus, we found a dopaminergic neuromodulatory effect that was highly specific with respect to neural frequency, latency, layer and tonotopic mapping. Consistent with the fact that mainly responses phase-locked to the stimulus are retained by trial averaging of time-series as it is carried out for the evoked responses, a corresponding neuromodulatory effect was also found in the evoked power spectrum in the same layer and at the same frequencies with a peak of the effect

at 94 Hz. Dopaminergic neuromodulation of oscillatory response amplitudes in the high gamma-band, however, was less pronounced than the modulation of stimulus phase-locking. SKF-38393 treatment did not significantly increase stimulus-induced power relative to silent background in the high gamma-band, although there was a significant decrease after application of antagonist SCH-23390 between 62 and 100 Hz.

For induced background power spectra, only non-antagonistic effects of SKF-38393 and SCH-23390 were found. These effects were independent of stimulation and occurred even during the pause. Moreover, these effects showed up as constant offsets over time in time-frequency analysis and therefore apparently reflected tonic changes in cortical background state. Broad high-frequency changes might therefore indicate changes in spontaneous neural background noise. In particular, broadband induced background power was increased after SKF-38393 application at frequencies above 10 Hz in layers I/II and was decreased in a broad band from 6 to 54 Hz in layer Vb. With SCH-23390 application induced background power further decreased in layer V and showed an additional decrease at low frequencies from 3 to 14 Hz in layer VI. Notably, no changes in background power occurred in layer III/IV, where stimulus-related changes in phase-locking and power were found.

Methodological considerations

The antagonistic pattern of change with consecutive administration of SKF-38393 and SCH-23390, as well as the high stimulus specificity, makes it unlikely that dopaminergic neuromodulation of

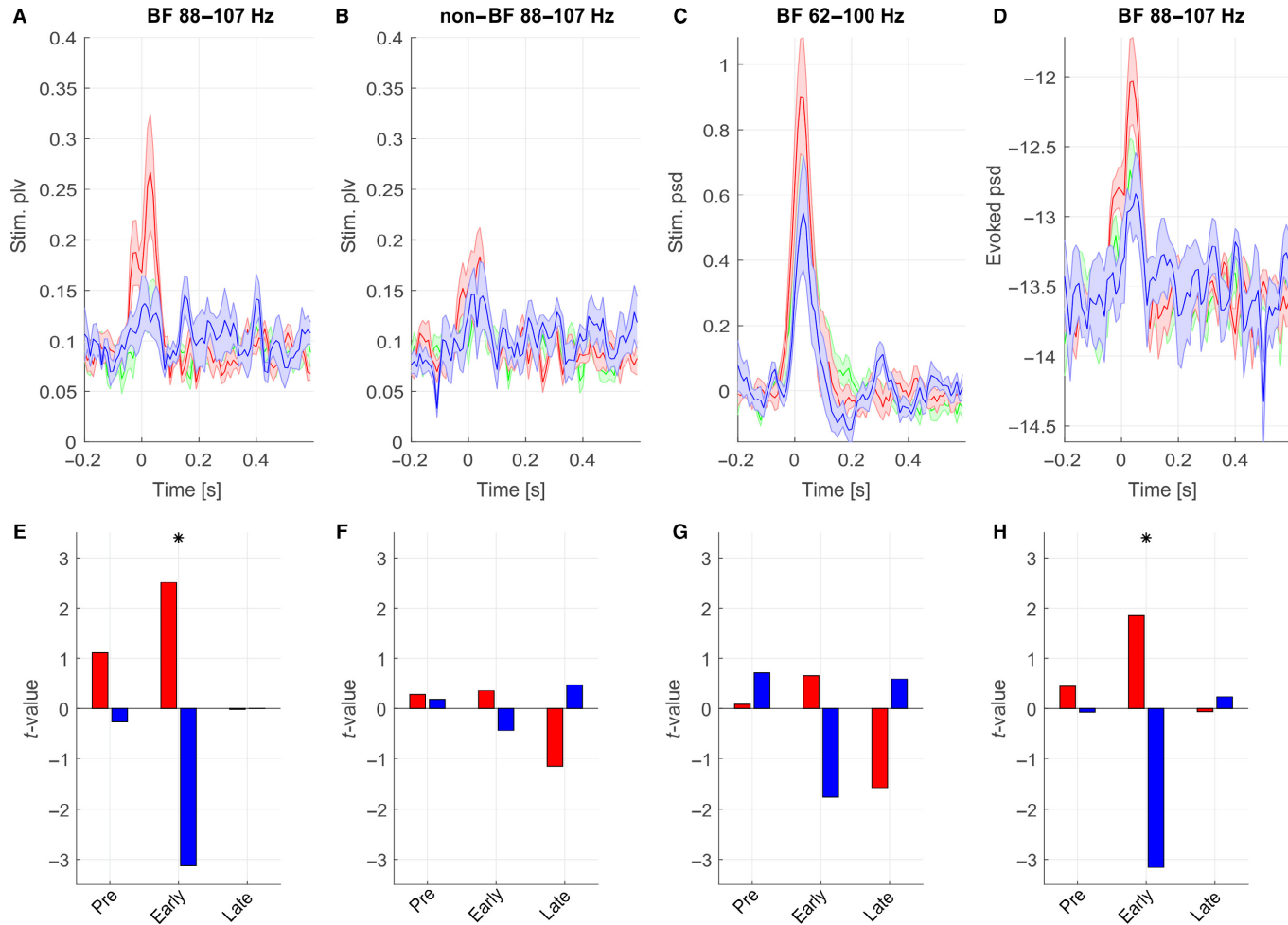


FIG. 7. Time-course of analytic stimulus phase-locking and stimulus-induced analytic power derived from FIR band-pass filtering and Hilbert transformation for the BL (green), after subsequent SKF-38393 (red) and SCH-23390 (blue) treatment in layers III/IV. Shown are grand mean and standard errors for frequency bands and layers with significant effects in multitaper spectral analysis. (A) High gamma stimulus phase-locking in the frequency range of antagonistic dopaminergic neuromodulation between 88 and 97 Hz in response to BF stimulation. (B) High gamma stimulus phase-locking between 88 and 97 Hz after non-BF stimulation. (C) High gamma stimulus-induced power between 62 and 100 Hz after BF stimulation. (D) Evoked high gamma power (89–96 Hz) after BF stimulation. Corresponding statistical *t*-values of SKF-38393 vs. BL (red) and SCH-23390 (blue) for the medians in a pre-stimulus (−200 to −50 ms), an early (0 to 50 ms) and a late (50 to 400 ms) time window of high gamma stimulus phase-locking at BF (E) and non-BF (F), and for high gamma stimulus-induced power at BF (G), and for evoked high gamma power at BF (H). Asterisks indicate significant neuromodulatory effects of the contrast (SKF-38393—BL)—(SCH-23390—SKF-38393) in a time window.

high gamma phase-locking reflects merely temporal effects of prolonged anesthesia. However, as there was no antagonistic pattern of change for the induced background power after consecutive administration of SKF-38393 and SCH-23390, it cannot be ruled out that the observed broadband and low-frequency effects might be due or at least be partially confounded by temporal changes related to anesthesia. Ketamine used for anesthesia in our study has been shown to alter neuronal oscillations in for instance lower frequencies (Blain-Moraes *et al.*, 2014) or higher frequency ranges (Lazarewicz *et al.*, 2009; Slovik *et al.*, 2017). Ketamine anesthesia has been shown to reduce NMDA-mediated synaptic input to inhibitory interneurons, as well as to pyramidal neurons, and by this contribute to the observed effects. Importantly, however, ketamine has been shown to affect D2-like dopamine receptors, but to have less pronounced effects on D1 receptors (Li *et al.*, 2015). Indeed, D1 agonists have been demonstrated to antagonize the ketamine-induced effects of cognitive impairment in marmosets (Nakako *et al.*, 2013). Hence, potential effects of ketamine anesthesia might have rather led us to

underestimate the network effect of D1-based dopamine. Although we cannot exclude that NMDA-related processes might influence the effects of dopamine in cortex, our goal was a CSD-based synaptic circuit analysis of the effects of D1/D5-activation using agonist SKF38393 and antagonist SCH-23390. To which degree induced power effects are based on dopaminergic neuromodulation, prolonged anesthesia or an interaction of both, requires further analysis.

High- and low gamma oscillations in neocortex

The dopaminergic neuromodulatory effect demonstrated in our study was found in the high gamma-band between 88 and 97 Hz. A dopamine-induced change in the high gamma-band has been found in LFP recorded from primary motor cortex as a long-term effect of L-dopa treatment (Dupre *et al.*, 2016). Less is known about dopaminergic neuromodulation of high gamma oscillations in sensory neocortex. High gamma oscillations (>60 Hz) have been observed intracranially in LFPs, and EcoGs, and non-invasively in

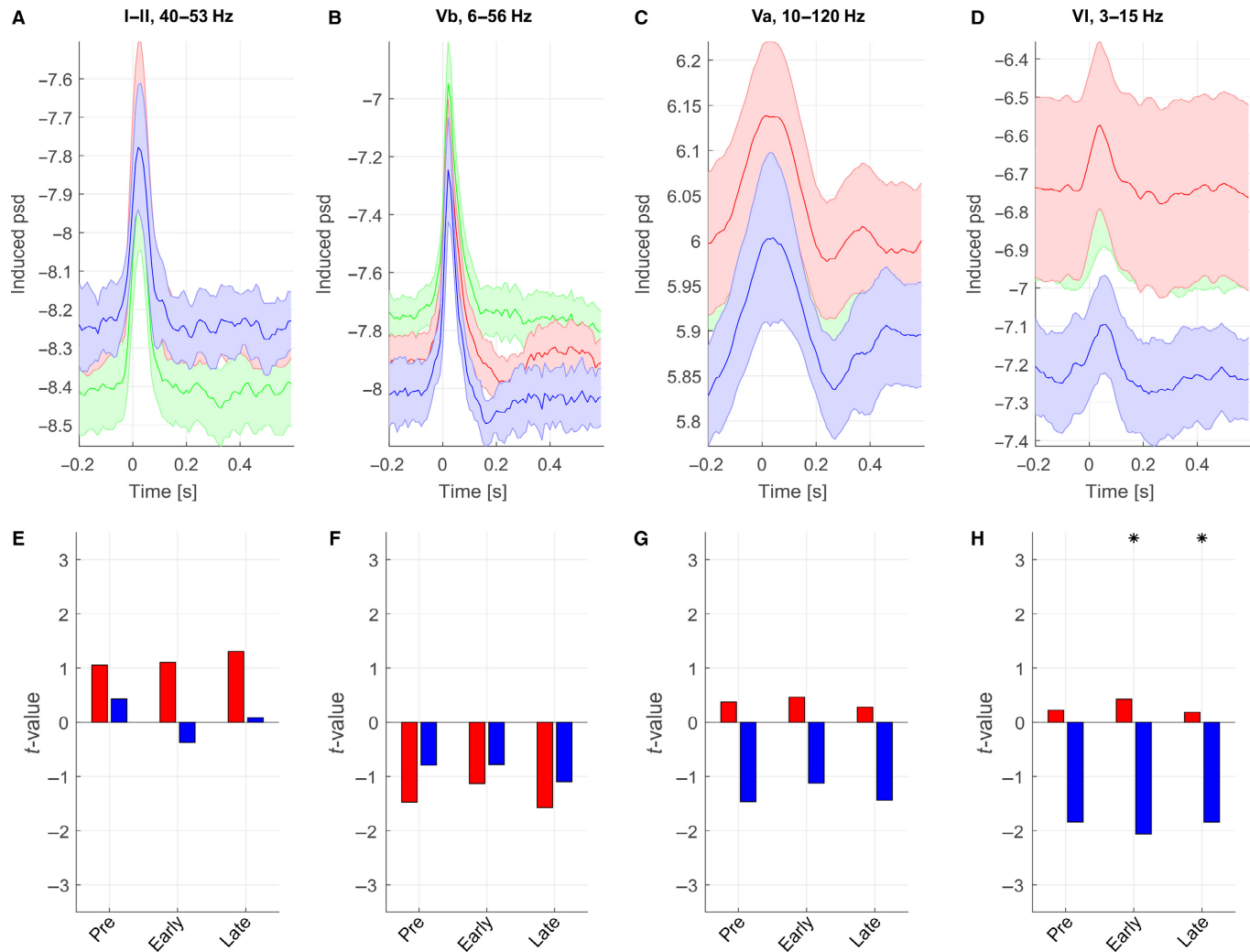


FIG. 8. Time-course of induced analytic power derived from FIR band-pass filtering and Hilbert transformation for the BL (green), after subsequent SKF-38393 (red) and SCH-23390 (blue) treatment at BF. Shown are grand mean and standard errors for frequency bands and layers with significant effects in multi-taper spectral analysis. (A) Layers I/II induced broadband power between 40 and 53 Hz after BF stimulation. (B) Layer Vb induced power between 6 and 54 Hz after BF stimulation. (C) Layer Va broadband induced power between 10 and 120 Hz in response to BF stimulation. (D) Layer VI low-frequency induced power between 3 and 14 Hz after BF stimulation. Corresponding Statistical *t*-values of SKF-38393 vs. BL (red) and SCH-23390 vs. SKF-38393 (blue) for the medians in a pre-stimulus (-200 to -50 ms), an early (0 to 50 ms), and a late (50 to 400 ms) time window of layers I/II induced broadband power (E), layer Vb induced power (F), layer Va broadband induced power (G), and layer VI low-frequency induced power between (H). Asterisks indicate significant neuromodulatory effects of the contrast (SKF-38393 – BL) – (SCH-23390 – SKF-38393) in a time window.

EEG/MEG measurements in humans and animals in many sensory cortical areas (for review, see Crone *et al.*, 2011) including auditory cortex (Crone *et al.*, 2001; Brosch *et al.*, 2002; Steinschneider *et al.*, 2008; Dürschmid *et al.*, 2016). For LFPs, as measured in our study, it has been shown that high gamma-activity shows a strong correlation with population spiking in its time-course, as well as across trials; high gamma activity is highly stimulus-specific, is spatially confined and rather reflects local synchronization of neurons than increases in firing rate (Ray *et al.*, 2008). In the visual cortex of the anesthetized cat, Herculano-Houzel *et al.* (1999) investigated high-frequency gamma oscillations in response to visual stimuli. With electric stimulation of the ascending mesencephalic reticular activating system (ARAS), they found gamma-responses between 70 and 105 Hz at stimulus onset with minimal central activation and temporally more prolonged low-frequency gamma oscillations between 20 and 65 Hz at higher levels of central activation. They attributed high gamma-responses (70–105 Hz) to thalamo-cortical input giving rise intracortical synchronization expressed at lower

frequencies (20–65 Hz). Phase-locking to stimulus onset, high layer and stimulus specificity, and short latencies strongly suggest stimulus-driven thalamo-cortical generators for the high gamma oscillations in our study. However, by CSD analysis of LFPs in slices of rat visual cortex in vitro, that is, in isolation from the thalamus, Oke *et al.* (2010) also found high gamma oscillations >70 Hz in superficial layers that consisted of rhythmic sink-source sequences in layer III. This fast gamma-oscillation coexisted with independent low gamma oscillations (30–70 Hz) in deep layers V/VI. Pharmacological analysis showed that these oscillations relied on synaptically generated sources and sinks generated from recurrent inhibition within intracortical microcircuits.

Physiological mechanisms and functional role of high gamma-oscillations

The exact physiological mechanisms leading to high gamma oscillations as those found in our study are still not resolved. High gamma

oscillations might be of synaptic origin and a property of circuits, but also might reflect more directly transient source and sink of spike generation. In both cases, high gamma oscillations are highly dependent on temporal synchronization of local neuron population and are therefore more sensitive to neural synchrony than to an increase in firing rate (Herculano-Houzel *et al.*, 1999; Ray *et al.*, 2008). This might explain, why we mainly found an effect in stimulus phase-locking, and only much weaker effects on stimulus-induced power. Several other studies have described stimulus phase-locking of gamma-responses, also called evoked gamma-responses, but have mainly found them in the low gamma range <70 Hz, e.g., in LFP recordings from auditory cortex of gerbils (e.g., Jeschke *et al.*, 2008), as well as in the electromagnetic field on the human scalp (Lenz *et al.*, 2008; Herrmann *et al.*, 2010). Compared to gamma-effects in our study, evoked gamma-band responses in these studies occur at longer latencies of 70–100 ms and lower frequencies.

Also, the functional role of high gamma oscillations is not well understood. Among other things, high gamma oscillations have been related to selective attention (Vidal *et al.*, 2006). Particularly, the alignment of gamma phase, as observed in our study, might align phases of high and low excitability relative to the temporal structure of the stimulus and by this facilitate extraction of relevant features (Lakatos *et al.*, 2007). Most importantly, gamma-band responses have been shown to increase, when stimuli are salient and behaviorally relevant (Herrmann *et al.*, 2010), and are target of a rapidly acting anticipatory top down modulation of stimulus responses (Schadow *et al.*, 2009). Recording LFPs from rat auditory cortex, Noda *et al.* (2017) showed that stimulus phase-locking in the gamma-band immediately increased, when stimulation was switched from unpredictable to temporally regular sequences. It is therefore hypothesized that early evoked gamma-band responses reflect prediction errors (Malmierca *et al.*, 2015; Dürschmid *et al.*, 2016). This fits well to our finding that dopaminergic modulation by D1/D5-receptor agonist SKF-38393 facilitated stimulus-specific phase-locking in the high gamma-band.

Possible physiological mechanisms and functional role of dopaminergic neuromodulation of high gamma stimulus phase-locking

In a former analysis (Happel *et al.*, 2014), we have demonstrated a dopamine-induced increase in infragranular synaptic current flow in layers Vb and VI relative to supragranular layers especially within an initial phase after stimulus onset. The analysis of the stimulus-induced spectra did not show large amplitude effects. Notably, spectral analysis is carried out on a different temporal scale: Whereas in Happel *et al.*, 2014; peak events were analyzed, spectral analysis and even time-frequency analysis in the current study provide information about oscillatory structures with durations on the order of several tens to several hundreds of ms.

In Happel *et al.* (2014), we further suggested the existence of a dopamine-modulated recurrent cortico-thalamo-cortical feedback loop that enhances thalamo-cortical reverberation which recruits horizontal cortico-cortical association networks in supragranular layers finally reading out and interpreting the sensory input. Enhanced recurrent cortico-thalamo-cortical feedback would be an ideal substrate for mediating dopamine-dependent phase-resetting as found in our study. As demonstrated by intracortical microstimulation and cross-laminar correlation analysis (Happel *et al.*, 2014), the delay of the limb from infragranular cortico-thalamic output back to layer IV thalamo-cortical input was about 6 ms. Stimulus phase-resetting between 88 and 97 Hz with a peak at 93 Hz could be mediated by

a loop with a delay of 10–12 ms (11 ms at the peak). Closing the loop from layer IV to layer V via additional synaptic relays would add a delay of several milliseconds. The dopamine-modulated cortico-thalamo-cortical feedback could therefore be the anatomical and physiological basis of the observed dopamine-modulated phase-resetting found in the present study.

An increase in thalamo-cortical synchronization at stimulus onset by dopamine might then facilitate the activation of supragranular intracortical networks, as it is reflected by a more sustained cortical activation, and by enhanced relative residuals as a measure of lateral input (Happel *et al.*, 2014). Activation of supragranular networks might then give rise to non-phase-locked low-frequency gamma oscillations (<60 Hz), which are generated by intracortical interactions, and are modulated by reticular thalamic input but not driven by geniculocortical input (Barth & MacDonald, 1996). As has been shown for the awake animal, these low-frequency gamma oscillations then can form spatial amplitude patterns with learning, which last for 100s of ms, and are associated rather with individually learned stimulus categories, than with physical properties of the stimuli themselves (Ohl *et al.*, 2001; Deliano *et al.*, 2009).

Supporting Information

Additional supporting information can be found in the online version of this article:

Fig. S1. (A) Representative example of averaged evoked CSD distributions in response to BF stimulation (left), nonBF-stimulation (middle) and pause (right) condition at baseline BL (top) and after injection (i.p.) of D1/D5-receptor agonist SKF-38393 (bottom). (B) Individual tuning-curves of RMS amplitudes of the granular layer III-IV sink of all animals ($n = 8$) at baseline BL (green) and after injection (i.p.) of D1/D5-receptor agonist SKF-38393 (red) and D1/D5 antagonist SCH-23390 (blue).

Fig. S2. Standardized differences of induced power spectra for nonBF-stimulation (light green) and during pause condition (dark green) expressed as t -values contrasted between SKF-38393 and BL (A), and between SCH-23390 and SKF-38393 (B). Power spectra were log-transformed for each taper on the single-trial level. Standardization was based on sample means and standard errors of the mean across subjects ($n = 8$ for BL vs SKF-38393, $n = 5$ for SCH-23390 vs SKF-38393) and tapers ($n_t = 5$). Asterisks mark Bonferroni-corrected significant differences in the corresponding color. For details, see Materials and Methods.

Fig. S3. Standardized differences of stimulus phase-locking (red), and stimulus-induced power (blue) spectra for nonBF-stimulation expressed as t -values contrasting SKF-38393 and BL (A), and SCH-23390 and SKF-38393. Power spectra were log-, and phase-locking spectra logit-transformed for each taper, on the single-trial and on the single-subject level, respectively. Standardization was based on sample means and standard errors of the mean across subjects ($n = 8$ for BL vs SKF-38393, $n = 5$ for SCH-23390 vs. SKF-38393) and tapers ($n_t = 5$). Asterisks mark Bonferroni-corrected significant differences in the corresponding color. For details, see Materials and Methods.

Acknowledgements

We are grateful to Kathrin Ohl for expert technical assistance during animal surgery and histological analysis of electrode localizations. This work was supported by grants from the Deutsche Forschungsgemeinschaft (DFG) and the Leibniz Association (WGL).

Conflict of interest

The authors declare no competing financial interests.

Data accessibility

The data are available on request to the corresponding author for researchers who meet the criteria for access to confidential data without limitations.

Author contributions

FWO conceived the study; MD, MFKH and FWO designed the experimental strategy; MD, MGKB and MET carried out data analysis; MD developed and carried out statistical test procedures; MGKB and MMZ performed electrophysiological measurements; MFKH supervised electrophysiological experiments; MD, MGKB, MFKH and FWO wrote the article with the help of all other coauthors.

References

- Barth, D.S. & MacDonald, K.D. (1996) Thalamic modulation of high-frequency oscillating potentials in auditory cortex. *Nature*, **383**, 78–81.
- Blain-Moraes, S., Lee, U., Ku, S., Noh, G. & Mashour, G.A. (2014) Electrocorticographic effects of ketamine on power, cross-frequency coupling, and connectivity in the alpha bandwidth. *Front. Syst. Neurosci.*, **8**, 1–9.
- Bokil, H., Andrews, P., Kulkarni, J.E., Mehta, S. & Mitra, P.P. (2010) Chronux : A platform for analyzing neural signals. *J. Neurosci. Methods*, **192**, 146–151.
- Bromberg-Martin, E.S., Matsumoto, M. & Hikosaka, O. (2010) Dopamine in motivational control: rewarding, aversive, and alerting. *Neuron*, **68**, 815–834.
- Brosch, M., Budinger, E. & Scheich, H. (2002) Stimulus-related gamma oscillations in primate auditory cortex. *J. Neurophysiol.*, **87**, 2715–2725.
- Crone, N.E., Boatman, D., Gordon, B. & Hao, L. (2001) Induced electrocorticographic gamma activity during auditory perception. Brazier Award-winning article, 2001. *Clin. Neurophysiol.*, **112**, 565–582.
- Crone, N.E., Korzeniewska, A. & Franaszczuk, P.J. (2011) Cortical gamma responses: Searching high and low. *Int. J. Psychophysiol.*, **79**, 9–15.
- Deliano, M., Scheich, H. & Ohl, F.W. (2009) Auditory cortical activity after intracortical microstimulation and its role for sensory processing and learning. *J. Neurosci.*, **29**, 15898–15909.
- Dupre, K.B., Cruz, A.V., Mccoy, A.J., Delaville, C., Gerber, C.M., Katherine, W. & Walters, J.R. (2016) Effects of L-dopa priming on cortical high beta and high gamma oscillatory activity in a rodent model of Parkinson's disease. *Neurobiol. Dis.*, **86**, 1–15.
- Dürschmid, S., Edwards, E., Reichert, C., Dewar, C., Hinrichs, H., Heinze, H.-J., Kirsch, H.E., Dalal, S.S. *et al.* (2016) Hierarchy of prediction errors for auditory events in human temporal and frontal cortex. *Proc. Natl. Acad. Sci.*, **113**, 6755–6760.
- Freeman, W.J., Holmes, M.D., West, G.A. & Vanhatalo, S. (2006) Fine spatiotemporal structure of phase in human intracranial EEG. *Clin. Neurophysiol.*, **117**, 1228–1243.
- Groppe, D.M., Urbach, T.P. & Kutas, M. (2011) Mass univariate analysis of event-related brain potentials/fields II: Simulation studies. *Psychophysiology*, **48**, 1726–1737.
- Happel, M.F.K., Jeschke, M. & Ohl, F.W. (2010) Spectral Integration in primary auditory cortex attributable to temporally precise convergence of thalamocortical and intracortical input. *J. Neurosci.*, **30**, 11114–11127.
- Happel, M.F.K., Deliano, M., Handschuh, J. & Ohl, F.W. (2014) Dopamine-modulated recurrent corticoefferent feedback in primary sensory cortex promotes detection of behaviorally relevant stimuli. *J. Neurosci.*, **34**, 1234–1247.
- Herculano-Houzel, S., Munk, M.H., Neuenschwander, S. & Singer, W. (1999) Precisely synchronized oscillatory firing patterns require electroencephalographic activation. *J. Neurosci.*, **19**, 3992–4010.
- Herrmann, C.S., Fründ, I. & Lenz, D. (2010) Human gamma-band activity: A review on cognitive and behavioral correlates and network models. *Neurosci. Biobehav. Rev.*, **34**, 981–992.
- Jeschke, M., Lenz, D., Budinger, E., Herrmann, C.S. & Ohl, F.W. (2008) Gamma oscillations in gerbil auditory cortex during a target-discrimination task reflect matches with short-term memory. *Brain Res.*, **1220**, 70–80.
- Lakatos, P., Chen, C.M., O'Connell, M.N., Mills, A. & Schroeder, C.E. (2007) Neuronal oscillations and multisensory interaction in primary auditory cortex. *Neuron*, **53**, 279–292.
- Lazarewicz, M.T., Ehrlichman, R.S., Maxwell, C.R., Gandal, M.J., Finkel, L.H. & Siegel, S.J. (2009) Ketamine modulates theta and gamma oscillations. *J. Cogn. Neurosci.*, **22**, 1452–1464.
- Lenz, D., Jeschke, M., Schadow, J., Naue, N., Ohl, F.W. & Herrmann, C.S. (2008) Human EEG very high frequency oscillations reflect the number of matches with a template in auditory short-term memory. *Brain Res.*, **1220**, 81–92.
- Li, Y., Zhu, Z.R., Ou, B.C., Wang, Y.Q., Tan, Z.B., Deng, C.M., Gao, Y.Y., Tang, M. *et al.* (2015) Dopamine D2/D3 but not dopamine D1 receptors are involved in the rapid antidepressant-like effects of ketamine in the forced swim test. *Behav. Brain Res.*, **279**, 100–105.
- Malmierca, M.S., Anderson, L.A. & Antunes, F.M. (2015) The cortical modulation of stimulus-specific adaptation in the auditory midbrain and thalamus: a potential neuronal correlate for predictive coding. *Front. Syst. Neurosci.*, **9**, 1–14.
- Min, B.K., Busch, N.A., Debener, S., Kranczioch, C., Hanslmayr, S., Engel, A.K. & Herrmann, C.S. (2007) The best of both worlds: Phase-reset of human EEG alpha activity and additive power contribute to ERP generation. *Int. J. Psychophysiol.*, **65**, 58–68.
- Mitra, P.P. & Bokil, H. (2008) *Observed Brain Dynamics*. Oxford, New York: Oxford University Press.
- Mitzdorf, U. (1985) Current source-density method and application in cat cerebral cortex: investigation of evoked potentials and EEG phenomena. *Physiol. Rev.*, **65**, 37–100.
- Nakako, T., Murai, T., Ikejiri, M., Ishiyama, T., Taiji, M. & Ikeda, K. (2013) Effects of a dopamine D1 agonist on ketamine-induced spatial working memory dysfunction in common marmosets. *Behav. Brain Res.*, **249**, 109–115.
- Noda, T., Amemiya, T., Shiramatsu, T.I. & Takahashi, H. (2017) Stimulus phase locking of cortical oscillations for rhythmic tone sequences in rats. *Front. Neural. Circ.*, **11**, 1–13.
- Ohl, F.W., Scheich, H. & Freeman, W.J. (2000) Topographic analysis of epidural pure-tone – evoked potentials in gerbil auditory cortex. *J. Neurophysiol.*, **83**, 3123–3132.
- Ohl, F.W., Scheich, H. & Freeman, W.J. (2001) Change in pattern of ongoing cortical activity with auditory category learning. *Nature*, **412**, 733–736.
- Oke, O.O., Magony, A., Anver, H., Ward, P.D., Jiruska, P., Jefferys, J.G.R. & Vreugdenhil, M. (2010) High-frequency gamma oscillations coexist with low-frequency gamma oscillations in the rat visual cortex in vitro. *Eur. J. Neurosci.*, **31**, 1435–1445.
- Radtke-Schuller, S., Schuller, G., Angenstein, F., Grosser, O.S., Goldschmidt, J. & Budinger, E. (2016) Brain atlas of the Mongolian gerbil (*Meriones unguiculatus*) in CT/MRI-aided stereotaxic coordinates. *Brain Struct. Funct.*, **221**, 1–272.
- Ray, S., Crone, N.E., Niebur, E., Franaszczuk, P.J. & Hsiao, S.S. (2008) Neural correlates of high-gamma oscillations (60–200 Hz) in macaque local field potentials and their potential implications in electrocorticography. *J. Neurosci.*, **28**, 11526–11536.
- Rothe, T., Deliano, M., Scheich, H. & Stark, H. (2009) Segregation of task-relevant conditioned stimuli from background stimuli by associative learning. *Brain Res.*, **1297**, 143–159.
- Schadow, J., Lenz, D., Dettler, N., Fründ, I. & Herrmann, C.S. (2009) Early gamma-band responses reflect anticipatory top-down modulation in the auditory cortex. *NeuroImage*, **47**, 651–658.
- Schaefer, M.K., Kössl, M. & Hechavarria, J.C. (2017) Laminar differences in response to simple and spectro-temporally complex sounds in the primary auditory cortex of ketamine-anesthetized gerbils. *PLoS One*, **12**, e0182514.
- Schicknick, H., Schott, B.H., Budinger, E., Smalla, K.H., Riedel, A., Seidenbecher, C.I., Scheich, H., Gundelfinger, E.D. *et al.* (2008) Dopaminergic modulation of auditory cortex-dependent memory consolidation through mTOR. *Cereb. Cortex*, **18**, 2646–2658.
- Schicknick, H., Reichenbach, N., Smalla, K.-H., Scheich, H., Gundelfinger, E.D. & Tischmeyer, W. (2012) Dopamine modulates memory consolidation of discrimination learning in the auditory cortex. *Eur. J. Neurosci.*, **35**, 763–774.
- Slovik, M., Rosin, B., Moshel, S., Mitelman, R., Schechtman, E., Eitan, R., Raz, A. & Bergman, H. (2017) Ketamine induced converged synchronous gamma oscillations in the cortico-basal ganglia network of nonhuman primates. *J. Neurophysiol.*, **118**, 917–931.
- Stark, H., Rothe, T., Deliano, M. & Scheich, H. (2008) Dynamics of cortical theta activity correlates with stages of auditory avoidance strategy formation in a shuttle-box. *Neuroscience*, **151**, 467–475.

- Steinschneider, M., Fishman, Y.I. & Arezzo, J.C. (2008) Spectrotemporal analysis of evoked and induced electroencephalographic responses in primary auditory cortex (A1) of the awake monkey. *Cereb. Cortex*, **18**, 610–625.
- Thomas, H., Tillein, J., Heil, P. & Scheich, H. (1993) Functional organization of auditory cortex in the Mongolian Gerbil (*Meriones unguiculatus*). I. Electrophysiological mapping of frequency representation and distinction of fields. *Eur. J. Neurosci.*, **5**, 882–897.
- Vidal, J.R., Chaumon, M., O'Regan, J.K. & Tallon-Baudry, C. (2006) Visual grouping and the focusing of attention induce gamma-band oscillations at different frequencies in human magnetoencephalogram signals. *J. Cogn. Neurosci.*, **18**, 1850–1862.